A Three-Dimensional Kinematics Analysis of a Koi Carp Pectoral Fin by Digital Image Processing

Lei Wang[1], Min Xu[1], Bo Liu[1], Kin Huat Low[2], Jie Yang[1], Shiwu Zhang[1]

1. *Department of Precision Machinery and Precision Instrumentation, University of Science and Technology of China, Hefei, Anhui* 230026, *P. R. China*
2. *School of Mechanical and Aerospace Engineering, Nanyang Technological University, Singapore* 639798, *Singapore*

Abstract

Pectoral fins fascinate researchers for their important role in fish maneuvers. By possessing a complicated flexible structure with several fin rays made by a thin film, the fin exhibits a three-dimensional (3D) motion. The complex 3D fin kinematics makes it challenging to study the performance of pectoral fin. Nevertheless, a detailed study on the 3D motion pattern of pectoral fins is necessary to the design and control of a bio-inspired fin rays. Therefore, a highspeed photography system is introduced in this paper to study the 3D motion of a Koi Carp by analyzing the two views of its pectoral fin simultaneously. The key motions of the pectoral fins are first captured in both hovering and retreating. Next, the 3D configuration of the pectoral fins is reconstructed by digital image processing, in which the movement of fin rays during fish retreating and hovering is obtained. Furthermore, the method of Singular Value Decomposition (SVD) is adopted to extract the basic motion patterns of pectoral fins from extensive image sequences, i.e. expansion, bending, cupping, and undulation. It is believed that the movement of the fin rays and the basic patterns of the pectoral fins obtained in the present work can provide a good foundation for the development and control of bionic flexible pectoral fins for underwater propeller.

Keywords: highspeed photography, Singular Value Decomposition (SVD), three-dimensional kinematics, digital image processing

1 Introduction

Fishes are the earliest vertebrates in the world, which have evolved more than five hundred million years in nature. The high performance of fish swimming, such as great maneuverability, high efficiency and low noise, can be attributed to their shapes, structures and motion patterns. The swimming performance could inspire us for innovative ideas of improving underwater propeller.

Based on the roles of the body and fins in generating propulsion[1], fish swimming modes can be divided into two categories: Body and Caudal Fin (BCF) and Median and/or Paired Fin (MPF). Most fishes swim in BCF mode, while a few fishes use MPF mode[2]. The fish in MPF mode can obtain a higher stability and higher maneuverability, which implies that they can perform well in keeping body balance, retreating, hovering and turning movements. However, the fish by BCF mode can gain a larger propulsion force during escape and prey[3].

Researchers have conducted a variety of studies on the pectoral fins, including physiology, morphology and kinematics. By analyzing the electromyography (EMG) activity in abductors and adductors of pectoral fins together with the highspeed photography technology, Westneat[4] studied the propulsion mechanism of pectoral fins flapping. Walker *et al.*[5] observed the morphological parameters and swimming propulsion of myliobatiformes and compared the impact of the kinematic parameters of pectoral fins on swimming speed and propulsive performance. Yan *et al.*[6] investigated the morphological and mechanics parameters of a Koi Carp pectoral fin.

Pectoral fins have complex flexible structures composed of jointed bony supports that are under active

Corresponding author: Shiwu Zhang
E-mail: swzhang@ustc.edu.cn

control via pectoral fin musculature[7,8]. Therefore, the study of the fin kinematics is a challenging research. Lauder and Madden[9] and Flammang and Lauder[10] examined the hydrodynamics of highly deformable pectoral fin of a bluegill sunfish during steady forward swimming. Low *et al.* and Cai *et al.*[11,12] analyzed pectoral fin motions of labriform, rowing, flapping and feathering for the development of a bionic modular pectoral fin. Peng *et al.*[13], Drucker *et al.*[14] and Mittal *et al.*[15] adopted Digital Particle Image Velocimetry (DPIV) technology to study the 3D motion of pectoral fins, dorsal fin, and ventral fin of sunfish. They went on to acquire the propulsion force, lift force and lateral force of fins in different motion patterns. On the other hand, Bozkurttas *et al.*[16] developed low-dimensional models of the pectoral fins gait of sunfish based on a Proper Orthogonal Decomposition (POD). They also discussed the implications of the POD analysis and performance scaling on the design of a robotic pectoral fin.

The existing experimental research on the kinematics of pectoral fins mainly concerns the analysis of kinematic parameters in fish steady swimming[17–21]. Whereas pectoral fins play a more important role in fish maneuvers, especially during retreating and hovering[22]. How to obtain the motion patterns of pectoral fins during retreating and hovering is an important procedure in the design and control of a bio-inspired fin. Meanwhile, one might integrate the bio-inspired fin with a robotic fish or an underwater propeller to enhance the stability and maneuverability in propulsion[6,23–27].

The present work is concerned with the kinematics study on Koi Carp, whose swimming is a typical carangiform, possessing a great maneuverability and a high swimming efficiency. The good performance of Koi Carp is due to the pectoral fin, which can carry out complex, flexible and 3D motions. The fin movement of live fish during retreating and hovering are captured and analyzed by digital image processing. The method of Singular Value Decomposition (SVD)[28] is also used to extract basic motion patterns of the pectoral fin, including expansion, bending, cupping, and undulation.

2 Materials and methods

In order to investigate the 3D motions of pectoral fins, an experimental system is developed for the 3D kinematics of pectoral fins of Koi Carp. The kinematics of pectoral fins during retreating and hovering can be studied in details by digital image processing. As a consequence, the method of SVD is adopted to extract the basic patterns of pectoral fins.

2.1 Experimental system setup

The experimental setup consists of a transparent water tank, a mirror and a high-speed photography system, as shown in Fig. 1. The volume of the water tank is 90 cm × 45 cm × 35 cm in length, width and depth, respectively. A mirror placed at 45° was used to ensure the synchronization of a double perspective by using only a single camera. By this way, the top image is live fish, whereas the bottom image is the fish image on mirror. In the experimental system, we adopted a highspeed camera (CASIO, EX-F1), which can capture images up to 60 fps with the resolution of 2816 pixel × 2112 pixel. Two halogen lamps were used to guarantee sufficient light intensity in high-speed continuous shooting. A grid paper with the grid size of 10 mm × 10 mm was used as a reference base.
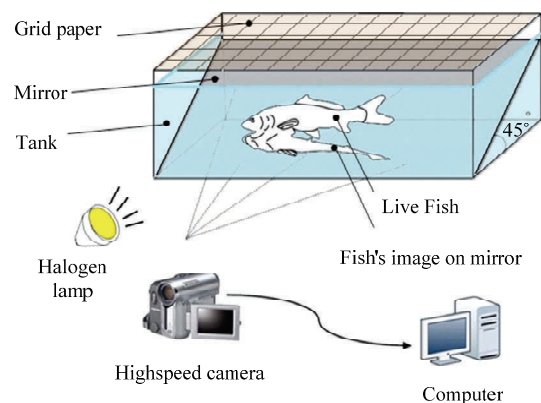
Fig. 1 Sketch of the experimental system.

The Koi Carp was housed in water with the temperature of 20°C±2°C. Several locations on the pectoral fins were marked before the experiment to facilitate the motion analysis of the pectoral fin. The concentration of 0.01 mL·L^{-1}–0.03 mL·L^{-1} 2-methylquinoline anesthesia was dropped into the clean water in another tank before marking the fin rays. The marking methods of aquatic animals including fluorescence labeling, Radio Frequency Identification Device (RFID), and color marker *in vitro*. In this experiment, we applied the color marker *in vitro*, which is an easy and reliable method to mark both sides (front and back) of the observed fin rays after the carp was deeply anesthetized. The marked points of

both sides should be aligned with the longitudinal axis of the fin ray, as shown in Figs. 2a and 2b. We can see from Fig. 2a that the pectoral fin of Koi Carp consists 14 fin rays, in which 20 black dots in one side of pectoral fin are marked points. The fin ray close to dorsal fin under neutral condition is dorsal leading ray; the pectoral fin close to ventral fin under neutral condition is ventral leading ray. The inner edge of pectoral fin is the part of pectoral fin close to the fish body, while the outer edge of pectoral fin is the part of pectoral fin away from the fish body.

(a)

(b)
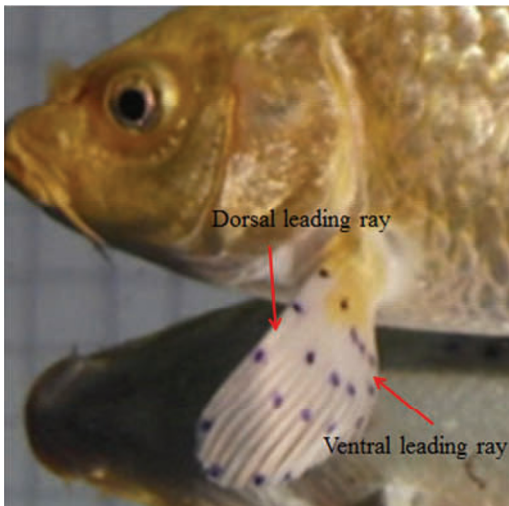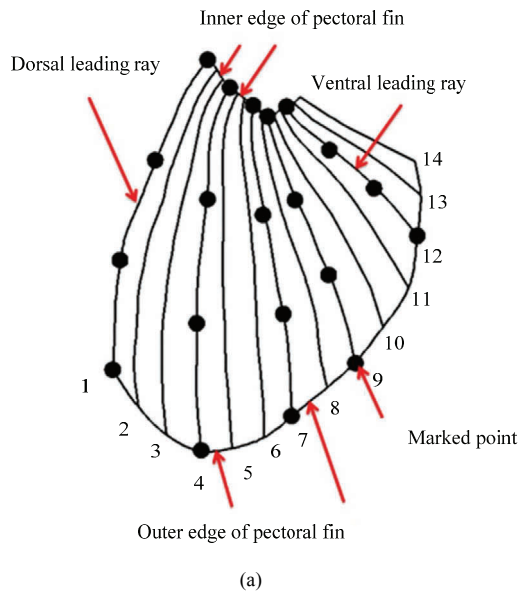
Fig. 2 Illustration of marked pectoral fin. (a) Model of the Koi Carp pectoral fin; (b) pectoral fin of live fish.

According to Shannon's sampling theorem[29], the phase difference of two adjacent sample points in a si-

nusoidal function must satisfy the requirement

$$\Delta\varphi \le \frac{\pi}{2}. \qquad (1)$$

The phase difference of two adjacent fin rays in a pectoral fin is given by

$$\Delta\varphi = \frac{2\pi n_\lambda}{n-1}, \qquad (2)$$

where n_λ is the wave number of undulation motion and n is the number of fin rays.

By combining Eqs. (1) and (2), one can obtain the relationship between the number of fin rays and wave number as

$$n \ge 4n_\lambda + 1. \qquad (3)$$

According to Eq. (3), at least five markers are required to simulate a complete cycle of undulation motion. In this work, five markers along the outer edge of fin rays (see Fig. 2a for the numbers of 1, 4, 7, 9, and 12) are selected. By extracting motion of the five marked points, the 3D motion profiles of the pectoral fins can be constructed by using digital image processing.

2.2 Coordinates setting for modeling

By using an inclined mirror in the experiment, we can obtain two views in each recording image. A fixed coordinate system $OXYZ$ is established as shown in Fig. 3, where X and Y are respectively along transparent tank length and width directions, while Z is along the direction perpendicular to the paper surface. $O'X'Y'Z'$ is a local coordinate system with the fish body. Note that X' direction is always from head to tail, Y' direction is always from dorsal leading ray to ventral leading ray along the height direction of the fish, and Z' direction is perpendicular to the fish body. The coordinate system $O''X''Y''Z''$ is obtained by translating $O'X'Y'Z'$ coordinates system. Note that β stands for the angle between coordinates X and X', α stands for the angle between coordinates Y and Y', and γ stands for the angle between coordinates Z and Z'. In view of the $O''X''Y''Z''$ coordinate system, θ, φ and δ respectively stand for the angles between the root of a fin ray (red line) and coordinates X'', Y'' and Z''.

The relationship between the two coordinate systems $OXYZ$ and $O'X'Y'Z'$ can be expressed in terms of rotation matrices as

$$\begin{pmatrix} X \\ Y \\ Z \end{pmatrix} = \begin{bmatrix} \cos\gamma & \sin\gamma & 0 \\ -\sin\gamma & \cos\gamma & 0 \\ 0 & 0 & 1 \end{bmatrix} \begin{bmatrix} \cos\beta & 0 & -\sin\beta \\ 0 & 1 & 0 \\ \sin\beta & 0 & \cos\beta \end{bmatrix} \begin{bmatrix} 1 & 0 & 0 \\ 0 & \cos\alpha & \sin\alpha \\ 0 & -\sin\alpha & \cos\alpha \end{bmatrix} \begin{pmatrix} X' \\ Y' \\ Z' \end{pmatrix} + \begin{pmatrix} X_{o1} \\ Y_{o1} \\ Z_{o1} \end{pmatrix}, \qquad (4)$$

where X_{o1}, Y_{o1} and Z_{o1} are the translation components.
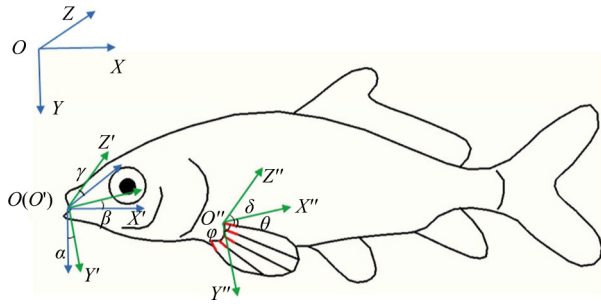
Fig. 3 A sketch of coordinate transformation.

For any point on fin ray, since two perspective images in one view share the same X' axis, X' coordinate and Y' coordinate of the projection point can be obtained in the front view, X' coordinate and Z' coordinate of the projection point can be obtained in the bottom view. Therefore, we are able to acquire the coordinates of the point in the *OXYZ* coordinate system by Eq. (4).

According to Ref. [30], the flexible fin ray has a bi-laminar structure with musculature attaching to the bases of the two hemitrichs. When the muscle tendon near the base of hemitrichs moves to one side, it causes a bending of the fin ray. This demonstrates the bilaminar structure of fin ray and their muscular control, which provides us a comprehensive understanding of the movement of the fin ray. The movement of fin ray is the result of muscle pulling force and hydrodynamic force. However, the root of fin ray is thicker than the tip, the stiffness is also larger. The deformation of the root of fin ray under hydrodynamic force is smaller than that of the tip. Thus, in order to capture the actual movement of live fish fin ray, we just study the root of fin ray. The root of fin ray performs a 2D motion, one is the motion within the plane, and the other is the motion perpendicular to the plane, as shown in Fig. 4. The movement of the root of fin ray is denoted by red line. Numbers 1, 4, 7, 9 and 12 are for the five respective marked fin rays (Fig. 2). The *X*, *Y* and *Z* axes are shown in Fig. 3. Note that λ is the angle between the fin ray and screen plane, η is the angle between the projection of the fin ray in the screen plane and *X* axis.
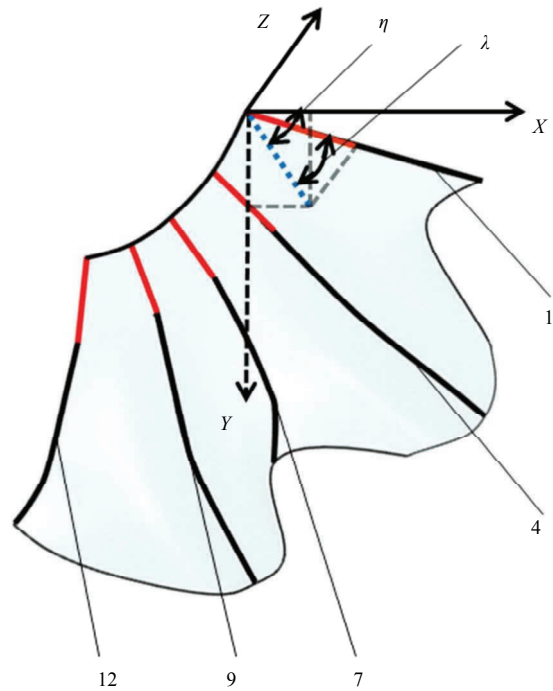
Fig. 4 The movement of the root of fin ray.

2.3 Image sequences process

The steps for image processing of pectoral fins motion are depicted in Fig. 5. A linear spatial filter is used to filter out the noise of raw images. Eq. (4) is used to transform the parameters between two coordinate systems. Image binaryzation is adopted to remove the undesired information from the color image. However, the binary image cannot identify each fin ray. The base of pectoral fin often stacks together, which makes the task challenging. To this end, morphological processing including dilation, erosion, opening and closing are used to separate different fin rays[31]. As presented in section **2.2**, for a point on the pectoral fin, the projections of a point in the front view and bottom view share the same *X* axis. Thus, we can gain the 3D coordinates of that point in the *OXYZ* coordinate system. We can then interpolate the 3D coordinate points to reconstruct the surface of the pectoral fins along span-wise and chord-wise direction, respectively. A detailed description of digital image processing flow can be found in Ref. [32].
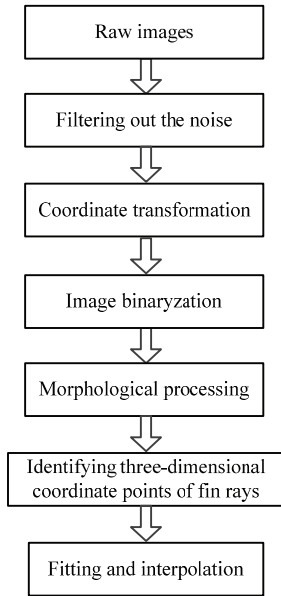
Fig. 5 Digital image processing flow.

2.4 SVD analysis of pectoral fin kinematics

SVD is a data analysis method used to find the hidden "mode(s)" in a large amount of data, which can be used in pattern recognition, data compression, *etc*. SVD is also adopted in a low order decomposition of a dynamic process[33].

Suppose G is an $m \times n$ matrix whose entries associated to the field K (either the field of real numbers or the field of complex numbers), there exists a factorization of the form:

$$G_{m \times n} = U_{m \times m} D_{m \times n} V^{*}_{n \times n}, \qquad (5)$$

where m represents the number of images in a retreating or hovering period, n represents 3D coordinates of q marked points; Note that U is an $m \times m$ unitary matrix over K, D is an $m \times n$ diagonal matrix with non-negative real numbers on the diagonal, and V^{*} is an $n \times n$ unitary matrix over K, which denotes the conjugate transpose of V. Such a factorization is called the singular value decomposition of G, i is the minimum value of m and n. The diagonal entries σ_i of D is known as the singular values of G.

By adopting $m = 9$ (number of pictures in one cycle) and $q = 20$ (number of marked points) in the present work, Eq. (5) can be expanded as

$$G_{9 \times 60} = \begin{bmatrix} X_1(t_1) & Y_1(t_1) & Z_1(t_1) & \cdots\cdots & X_{20}(t_1) & Y_{20}(t_1) & Z_{20}(t_1) \\ X_1(t_2) & Y_1(t_2) & Z_1(t_2) & \cdots\cdots & X_{20}(t_2) & Y_{20}(t_2) & Z_{20}(t_2) \\ \vdots & \vdots & \vdots & \vdots\ \vdots & \vdots & \vdots & \vdots \\ X_1(t_9) & Y_1(t_9) & Z_1(t_9) & \cdots\cdots & X_{20}(t_9) & Y_{20}(t_9) & Z_{20}(t_9) \end{bmatrix}.$$

A MATLAB program was employed to compute U, D, V^{*}. Therefore, the shape of any particular σ_i of D can be reconstructed according to Eq. (5)

$$G_K = UD_K V^{*}, \qquad (6)$$

where $K = 1, 2, \dots, 9$, and σ_i are arranged in descending order so that $\sigma_1 > \sigma_2 > \dots \sigma_9$. Diagonal matrix D can be can be expressed as

$$D_{9 \times 60} = \begin{bmatrix} \sigma_1 & 0 & \cdots & 0 & 0 & \cdots & 0 \\ 0 & \sigma_2 & \cdots & 0 & 0 & \cdots & 0 \\ \vdots & \vdots & \ddots & \vdots & 0 & \cdots & 0 \\ 0 & 0 & \cdots & \sigma_9 & 0 & \cdots & 0 \end{bmatrix}.$$

As a result, the Kth mode can be extracted by zeroing out all the singular values except for the Kth principal value, and reconstructing from the SVD according to Eq. (6). Finally, the time sequences of each mode can be calculated, which will be presented in section **3.2**.

3 Results and discussion

By observing the motion of Koi Carp in hovering or retreating, the pectoral fins move continuously, while other fins (dorsal fin, ventral fin, anal fin, and caudal fin) remaining nearly still. This implies that the pectoral fins play a vital role in retreating and hovering.

3.1 Movements of fin rays

By virtue of the digital image processing introduced in section **2.3**, the motion of fins was recorded during the experiment of fish retreating and hovering. For clarity, only one typical fin beat of the pectoral fin image sequences is presented next. The movements characteristic of fin rays are obtained by digital image processing of the captured photos, basic motion patterns of the pectoral fin in the two typical maneuvers can then be extracted from the image sequence by using SVD.

3.1.1 Retreating of fin rays

As shown in Fig. 6, the upper-row photos are taken from camera, while the lower-row images are the models generated from MATLAB. In every photo, the solid oval denotes real image in front view, whereas the dotted oval denotes image on mirror camera in bottom view. In the models below the photos, red lines represent the root of pectoral fin, blue lines represent the outer edge of pectoral fin, azury lines represent dorsal leading ray, and the green lines represent ventral leading ray. The snapshots

of the neighboring photos are in 50 ms time interval. The motion of pectoral fin during retreating is divided into two stages: in-stroke ($t = 0$, 0.05 s, 0.1 s, and 0.15 s), out-stroke ($t = 0.25$ s, 0.3 s, 0.35 s, and 0.4 s), while the result of $t = 0.2$ s is a transition posture from in-stroke to out-stroke. In the process of in-stroke, the pectoral fin contracts rapidly in order to reduce flapping surface, thus reducing resistance during retreating. In the process of out-stroke, the pectoral fin expands slowly relative to that in in-stroke to increase flapping surface, thus increasing retreating force.
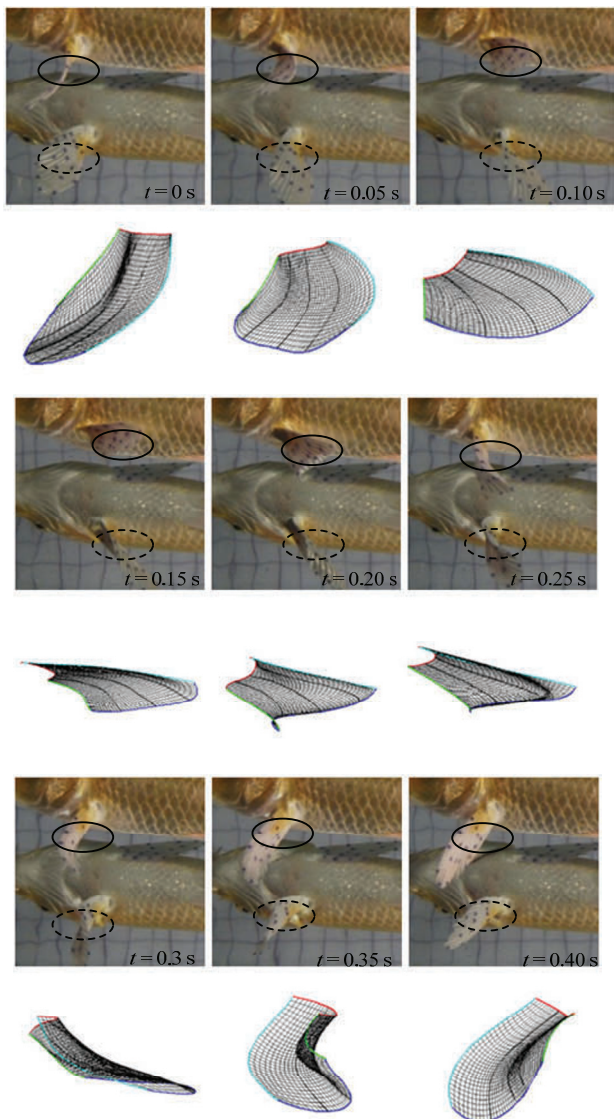
Fig. 6 Motion cycles of the pectoral fin during retreating.

Through extensive experimental observations of fin rays during retreating and hovering, the angles and deformed curves of dorsal leading ray during retreating can be obtained, as shown in Fig. 7. In Fig. 7a, the black dots,

red squares, and blue triangles represent the raw data obtained experimentally, whereas the results by the black curve, red curve and blue curve are generated by fourth-order polynomial fitting. The standard deviation of θ is 2.6 degrees, that of φ is 4.5 degrees, and that of δ is 5.0 degrees. The angles θ and φ can be divided into two distinct ranges according to in-stroke and out-stroke. In the process of in-stroke, θ decreases, whereas φ increases. In the process of out-stroke, θ gradually increases to the maximum value, whereas φ decreases to the value at $t = 0$ s. Note that δ does not change obviously. Fig. 7b presents the displacement of dorsal leading ray during retreating. The curves are obtained through the interpolation of the four marked points on fin rays, and the open circles denote the raw data obtained experimentally. The result shows that the dorsal leading ray moves only to one side, and the maximum displacement reaches 11.5 mm.
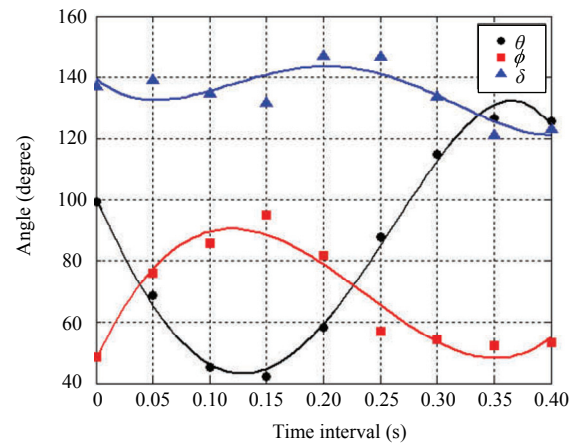
(a) Angles between the root of dorsal leading ray and the axes during retreating (see Fig. 3 for definitions of the angles).
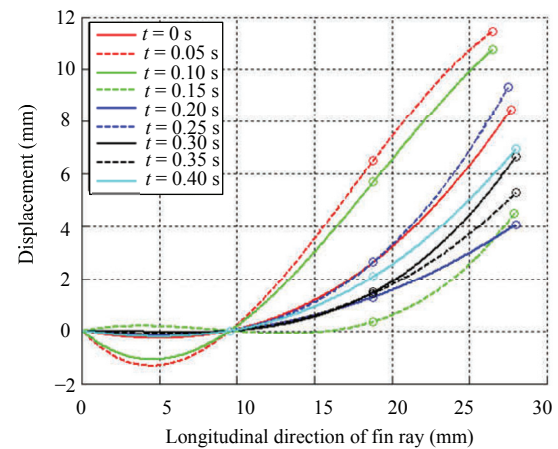
(b) Displacement of dorsal leading ray in a retreating cycle.
Fig. 7 Characteristic of dorsal leading ray during retreating.

Similarly, we can obtain the results for ventral leading rays, as shown in Fig. 8. In Fig. 8a, the standard deviation of θ is 6.0 degrees, that of φ is 5.2 degrees, and that of δ is 5.5 degrees. Note that θ and φ of ventral leading ray have the same characteristic as that of dorsal leading ray. However, δ increases quickly to 140 degrees before it decreases slowly. Ventral leading ray performs the movement in two opposite sides (Fig. 8b). This could be because the ventral leading ray is more flexible than the dorsal leading ray. The deformation of the ventral leading ray is larger at the time of 0.15 s, a transition time from in-stroke to out-stroke. This implies that the fin ray at the transition time withstands forces in two different directions.
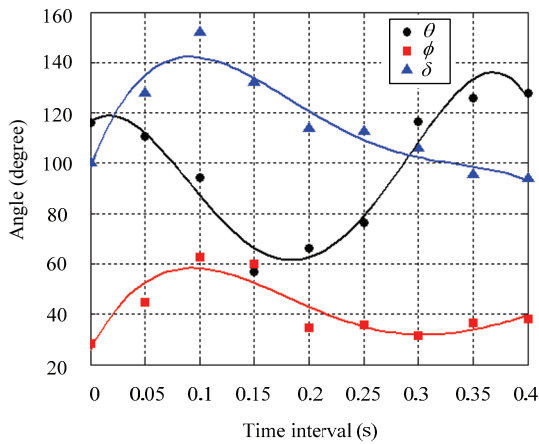
(a) Angles between the root of ventral leading ray and axes during retreating (see Fig. 3 for definition of the angles).
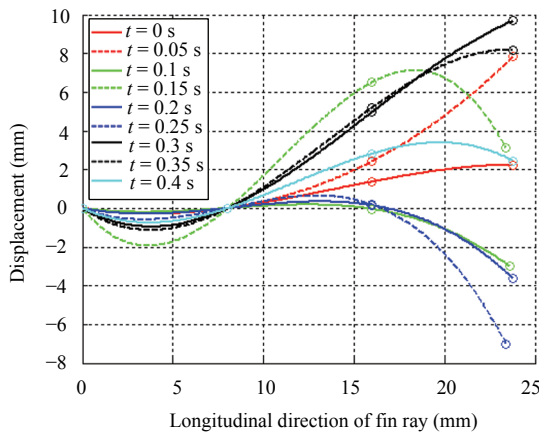
(b) Displacement of ventral leading ray in a retreating cycle.

Fig. 8 Characteristic of ventral leading ray during retreating.

Fig. 9 shows the angular movement of the marked fin rays during retreating. In Fig. 4, η and λ stand respectively for the angles of expansion and undulating of pectoral fin surface during retreating. In Fig. 9a, η can be divided into two distinct stages: from $t = 0$ s to $t = 0.15$ s, η decreases, from $t = 0.15$ s to $t = 0.4$ s, η increases, the surface area of pectoral fin in the stage is increasing. At $t = 0.15$s, the η of dorsal leading ray (Fin ray 1) reaches the minimum value 10 degrees, ventral leading ray (Fin ray 12) reaches 40 degrees. In a motion cycle, the relative change of η of dorsal leading ray and ventral leading ray reach 120 degrees and 80 degrees, respectively. Fig. 9b shows a delay of λ from Fin ray 1 to Fin ray 12 as the fin rays reach the maximum value. The relative change of λ of Fin ray 1 and Fin ray 12 can go up to 30 degrees and 50 degrees, respectively. This is because Fin ray 12 is softer than Fin ray 1. By studying the changes of η and λ, we can obtain expansion undulating angles of pectoral fin during retreating.
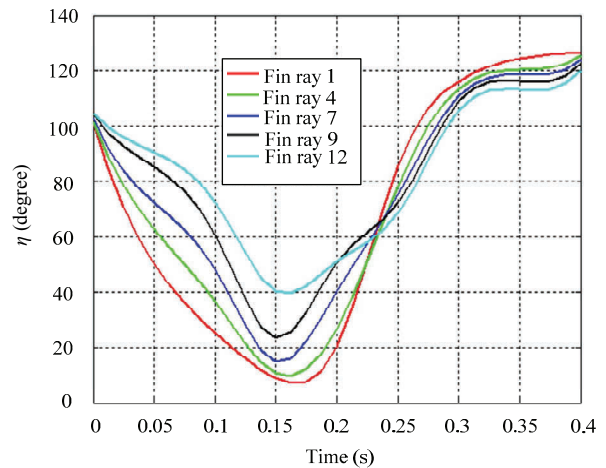
(a)
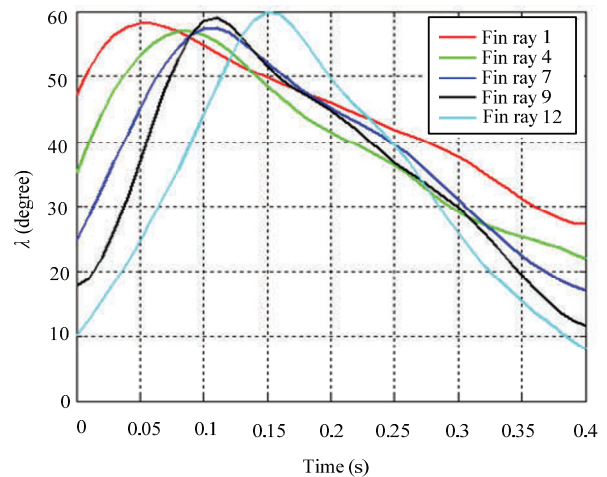
(b)

Fig. 9 Angle of the movement of marked fin rays during retreating. The curves are obtained by spline curve fitting. (a) η, (b) λ (see Fig. 2 for the position of the five marked fin rays; Fig. 4 for the definition of the angles).

3.1.2 Hovering of fin rays

The motion study of pectoral fins during hovering is also divided into two stages (as shown in Fig. 10), out-stroke (t = 0, 0.05 s, 0.1 s, 0.15 s) and in-stroke (t = 0.2 s, 0.25 s, 0.3 s, 0.35 s, 0.4 s). In the process of out-stroke, the pectoral fin expands suddenly to expand flapping surface before it gradually decreases. In the process of in-stroke, the pectoral fin expands slowly.
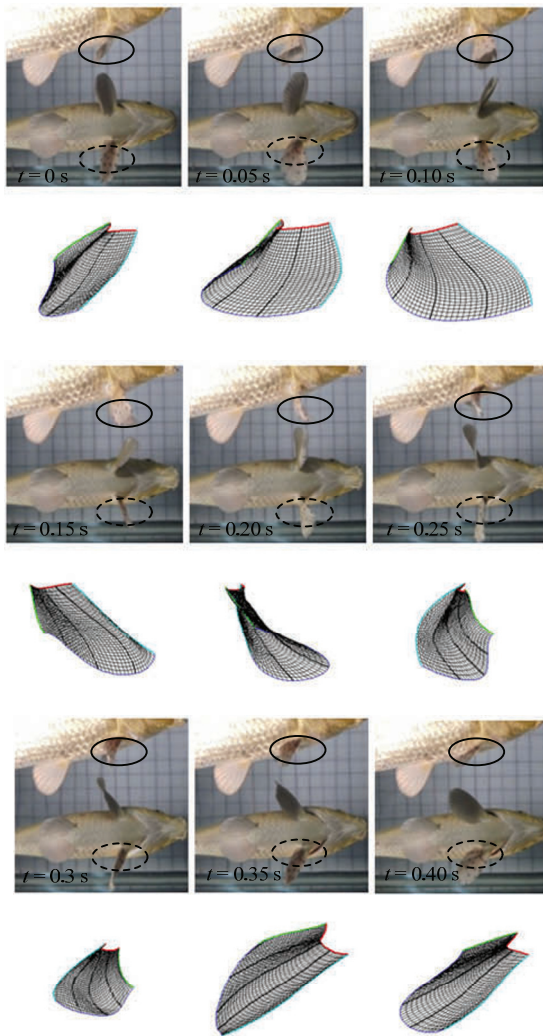
Fig. 10 Motion cycles of the pectoral fin during hovering.

Similarly to the method of the studying for fish retreating, we have obtained the results of Fig. 11 and Fig. 12 show the angles and displacements of dorsal leading ray and ventral leading ray in hovering (see Figs. 11 and 12). In Fig. 11a, the standard deviation of θ is 6.7 degrees, thate standard deviation of φ is 7.6 degrees, and thate standard deviation of δ is 4.7 degrees. The angle also can be divided into two distinct ranges according to in-stroke and out-stroke, θ and δ increase in the out-stroke, de-

crease in the in-stroke. However, the trend of φ is opposite. In Fig. 12a, the standard deviation of θ is 4.1 degrees, that of φ is 4.5 degrees, and that of δ is 2.8 degrees. The changing trend of φ and δ are consistent, decrease first and then increase. The minimum values are 20 degrees and 60 degrees, respectively. The maximum angle of θ approaches 90 degrees.

Fig. 11b shows the displacement of dorsal leading ray during hovering. It is seen that the dorsal leading ray only moves to one side, except at the time of 0.15 s. This implies that the fin ray withstands two different direction forces at the transition time. Fig. 12b shows similar trends as those in Fig. 11b. The ventral leading ray experiences larger deformation at the transition time of 0.1 s. Also, it is found that the deformation of ventral leading ray is larger than that of dorsal leading ray.
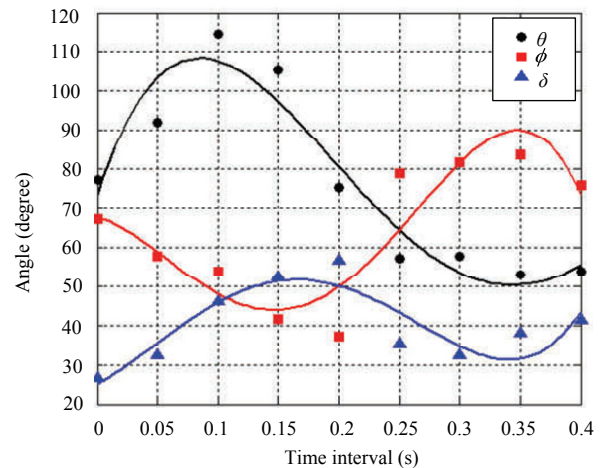
(a) Angles between the root of dorsal leading fin ray and axes during hovering (see Fig. 3 for definition of the angles).
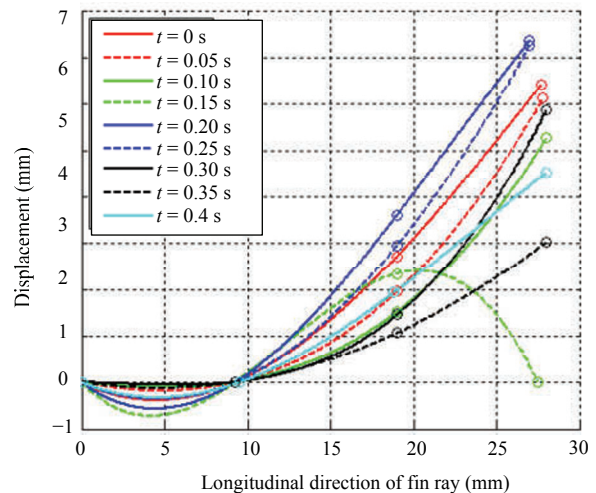
(b) Displacement of dorsal leading fin ray in a hovering cycle.

Fig. 11 Characteristic of dorsal leading fin ray during hovering.
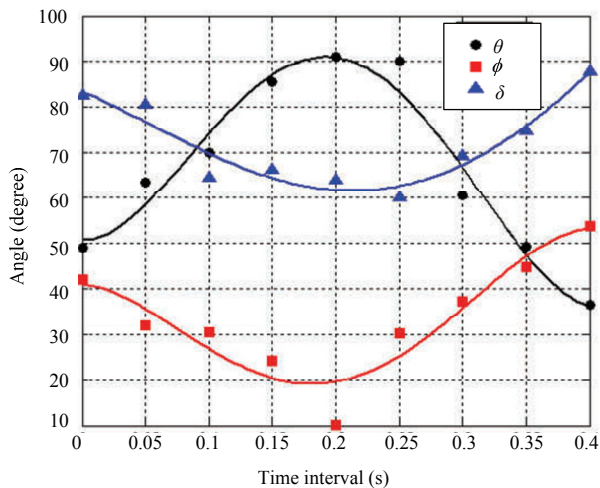
(a) Angles between the root of ventral leading ray and axes during hovering (see Fig. 3 for definition of the angles).
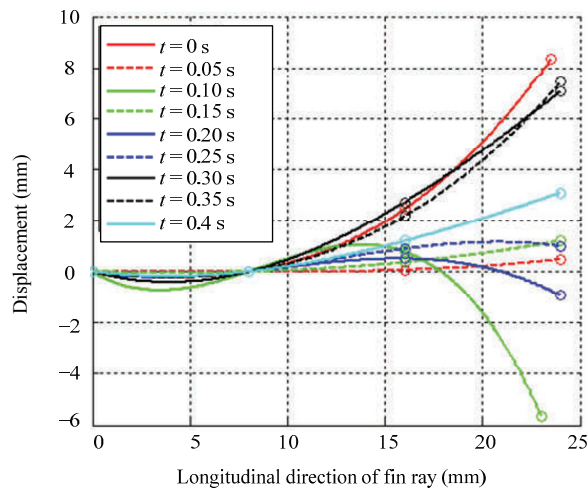
(b) Displacement of ventral leading ray in a hovering cycle.

Fig. 12 Characteristic of ventral leading ray during hovering.

(a)

(b)

Fig. 13 Angles of the movement of marked fin rays during hovering. The curves are obtained by spline curve fitting. (a) η, (b) λ (see Fig. 2 for the position of the five marked fin rays; Fig. 4 for the definition of the angles).

Fig. 13 shows the angular motions of marked fin rays during fish hovering. As depicted in Fig. 13a, the changes of η of dorsal leading ray (Fin ray 1) and Fin ray 12 reach 95 degrees and 45 degrees, respectively. There is a delay of λ when the fin rays reach their minimum values, as shown in Fig. 13b. The changes of λ of Fin ray 1 and Fin ray 12 are can both reach 25 degrees, smaller than that during retreating.

The location of the bio-inspired pectoral fin can be determined through θ, φ, and δ. The deformation of the flexible pectoral fin can be determined through the angular displacements of fin ray in terms of λ and η. The motion study of dorsal leading ray and ventral leading ray during retreating and hovering provides us a useful foundation for the design and control of the bio-inspired fin rays.

3.2 Motion analysis of pectoral fin

By virtue of MATLAB tri-mesh imaging, we can obtain the surface area of pectoral fin during retreating and hovering (see Fig. 14). The red dots and blue triangles are the raw data points obtained experimentally. The red curve is generated by fourth-order polynomial fitting. The standard deviation of surface area during hovering is 10.8 mm^2. Similarly, the blue curve is obtained by fourth-order polynomial fitting. The standard deviation of surface area during retreating is 7.0 mm^2. It is found from the result that the surface area of pectoral fin during retreating decreases in the process of in-stroke before the slow increase in the process of out-stroke. Moreover, the surface area of pectoral fin during hovering presents a cycle change in a fin beat. Accordingly, the Koi Carp is able to keep hovering and will not sink.
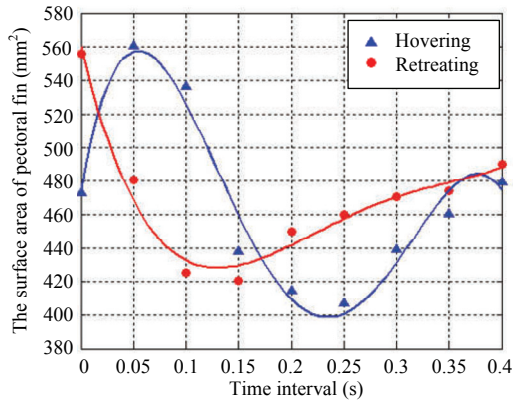
Fig. 14 Surface area of pectoral fins during hovering and retreating.

According to Eq. (6), the SVD analysis of fin kinematics results in nine distinct singular values during retreating and hovering. The singular values are normalized by the sum of all singular values, which are shown in Fig. 15. Note that the mode number is equal to the number of images extracted. It is worth-noting from Fig. 15 that the normalized singular value can be divided into two distinct regions, I: principal modes and II: residual modes. In region I, the normalized value of the first four modes (Modes 1 to 4) decreases rapidly. In region II, the normalized value of the five modes (Modes 5 to 9) keeps nearly constant. Fig. 15 shows that the first four modes (Modes 1 to 4) during retreating and hovering occupy above 90% of all nine modes. We can then conclude that the first four modes (both during retreating and hovering) represent the main features of the patterns of Koi Carp.
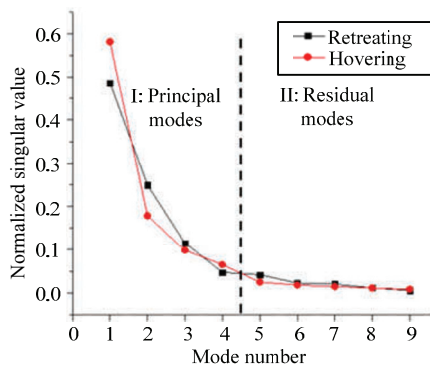
Fig. 15 SVD analysis of pectoral fin kinematics.

According to Eq. (6), the time sequences of each mode of retreating and hovering are calculated. It is found from the time sequences that the shape of each mode does not change much. For conciseness, only one

result is depicted in Fig. 16 for each mode of pectoral fin in retreating and hovering.
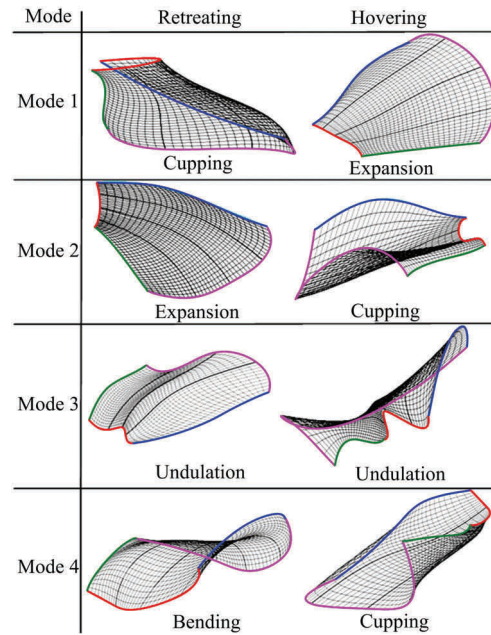
Fig. 16 First four modes of Koi Carp fin movement during retreating and hovering. The red line represent the root of pectoral fin, the pink line represent the outer edge of pectoral fin, the blue line represent dorsal leading ray, the green line represent ventral leading ray.

In Mode 1 of retreating shown in Fig. 16, the posture 'cupping', dorsal leading ray and ventral leading ray are in the same direction perpendicular to fin surface, which forms a cylindrical shape. In Mode 2 of retreating, the posture of 'expansion', dorsal leading ray and ventral leading ray move along the span-wise direction. The fin surface increases. Thus, the flapping surface also increases. In Mode 3 of retreating, the posture of 'undulation' and the whole fin surface presents a 'W' shape. The movement direction of adjacent fin rays is opposite, and the adjacent fin rays have phase difference. In Mode 4 of retreating, the posture of 'bending', fin rays bend and the fin surface displays parabolic.

In the four modes of retreating, the patterns of pectoral fins are obtained. According to the four modes of retreating, we can predict hovering motion modes on the basis of the motion analysis calculated from retreating. Mode 1 of hovering possesses similar shape to Mode 2 of retreating, as Mode 1 of hovering is also called 'expansion'. In Mode 2 of hovering, the dorsal leading ray and ventral leading ray are clearly separated, while the remaining fin rays are close to each other. The whole fin surface presents a 'Ω' shape, which is similar

to 'cupping'. Mode 3 of hovering that presents a 'W' shape is also called 'undulation'. Mode 4 of hovering possesses similar 'cupping' shape to Mode 1 of retreating.

Fig.17 presents Mode 5 of fin movement during retreating and hovering. Note that Modes 5 to 9 are the residual modes covered by Region II depicted in Fig. 15. The fin movement of Mode 5 during retreating becomes complex and irregular, which is difficult to describe the features of Mode 5. Furthermore, Mode 5 of hovering gets more complicated. The rest of the four modes (Modes 6 to 9) would become even more complicated than Mode 5. Thus, only the first four modes are depicted and analyzed for pectoral fin during retreating and hovering.
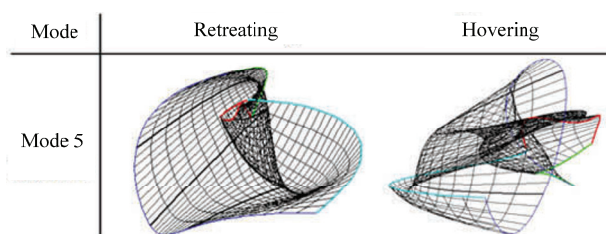
Fig. 17 Mode 5 of Koi Carp fin movement during retreating and hovering (see Fig. 16 for the definition of the color lines).

The four principal patterns of pectoral fins, namely expansion, bending, cupping, and undulation, are shown in Fig. 16. As it is challenging to simulate the motion of Koi Carp pectoral fins directly, the four basic patterns can provide an efficient method to simulate the motion of real pectoral fins. One can obtain arbitrary, complex 3D motions through the combination of two and more basic patterns.

4 Conclusions and future work

The experiments were carried out on a Koi Carp to record the spatial motion of pectoral fins. By using the MATLAB image from digital image processing, the kinematics of pectoral fins during retreating and hovering was studied. The motion of fin rays during fish retreating and hovering was studied, in which the expansion and undulating angles of pectoral fin surface were obtained. The motion of pectoral fins is complex and it is difficult to find directly the kinematic patterns of the pectoral fins. Therefore, SVD analysis of pectoral fins kinematics was suggested to find the hidden "mode(s)". Four basic patterns of pectoral fin were concluded in the present work.

The results demonstrate that the experimental system, the method of digital image process and the SVD analysis of pectoral fin kinematics provide a comprehensive technique of finding gait patterns of pectoral fins. The angles θ, φ and δ define the location of fin rays, while η and λ represent expansion and undulating angles of fin rays. The results and the identified four basic patterns of pectoral fins provide a good foundation for the development of bio-inspired fins.

In the future work, the proposed experimental system and the method of SVD can be adopted to analyze the complex kinematics of spatial fins, including cruising, turning, ascending, and descending, *etc*. More basic patterns can also be obtained in future works.

Acknowledgments

References

[1] Videler J J. *Fish Swimming*. Chapman & Hall, London, UK, 1993.

[2] Zhang Y, He J, Zhang G. Measurement on morphology and kinematics of crucian vertebral joints. *Journal of Bionic Engineering*, 2011, **8**, 10–17.

[3] Tangorra J L, Davidson S N, Hunter I W, Madden G A, Lauder G V, Dong H, Bozkurttas M, Mittal R. The development of a biologically inspired propulsor for unmanned underwater vehicles. *Journal of Oceanic Engineering*, 2007, **32**, 533–550.

[4] Westneat M W. Functional morphology of aquatic flight in fishes: kinematics, electromyography, and mechanical modeling of labriform locomotion. *American Zoologist*, 1996, **36**, 582–598.

[5] Walker J A, Westneat M W, Sandberg W C, Ramamurti R, Rosenberger L. Kinematics, dynamics, energetics, performance, ecomorphology of rowing and flapping propulsion. *American Zoologist*, 2001, **41**, 1618–1619.

[6] Yan Q, Wang L, Liu B, Yang J, Zhang S. A novel implementation of a flexible robotic fin actuated by shape memory alloy. *Journal of Bionic Engineering*, 2012, **9**, 156–165.

[7] Lauder G V, Drucker E G. Morphology and experimental hydrodynamics of fish fin control surfaces. *IEEE Journal of Oceanic Engineering*, 2004, **29**, 556–571.

[8] Webb P W. Stability and maneuverability. *Fish Biomechanics*, 2006, **23**, 281–332.

[9] Lauder G V, Madden G A. Fish locomotion: Kinematics and hydrodynamics of flexible foil-like fins. *Experiments in Fluids*, 2007, **43**, 641–653.

[10] Flammang B E, Lauder G V. Speed-dependent intrinsic caudal fin muscle recruitment during steady swimming in bluegill sunfish, *Lepomis macrochirus. The Journal of Experimental Biology*, 2008, **211**, 587–598.

[11] Low K H, Prabu S, Pattathil A P. Initial prototype design and development of hybrid modular under water vehicles. *IEEE International Conference on Robotics and Biomimetics*, Kunming, China, 2006, 311–316.

[12] Cai Y, Bi S, Low K H, Zhang L, Zong G. Posture analysis and application of a bionic pectoral foil. *IEEE International Conference on Robotics and Biomimetics*, Phuket, Thailand, 2011, 1783–1788.

[13] Peng J F, John O D, Madden G A, Lauder G V. Noninvasive measurement of instantaneous forces during aquatic locomotion: a case study of the bluegill sunfish pectoral fin. *The Journal of Experimental Biology*, 2007, **210**, 685–698.

[14] Drucker E G, Lauder G V. Wake dynamics and locomotor function in fishes: Interpreting evolutionary patterns in pectoral fin design. *Integrative and Comparative Biology*, 2002, **42**, 997–1008.

[15] Mittal R, Dong H, Bozkurttas M, Lauder G V, Madden G A. Locomotion with flexible propulsors: II. Computational Modeling of Pectoral Fin Swimming in Sunfish. *Bioinspiration & Biomimetics*, 2006, **1**, S35–S41.

[16] Bozkurttas M, Mittal R, Dong H, Lauder G V, Madden G A. Low-dimensional models and performance scaling of a highly deformable fish pectoral fin. *The Journal of Fluid Mechanics*, 2009, **631**, 311–342.

[17] Wu G. Measuring the three-dimensional kinematics of a free-swimming koi carp by video tracking method. *Journal of Bionic Engineering*, 2010, **7**, 49–55.

[18] Sitorus P, Nazaruddin Y, Leksono E, Budiyono A. Design and implementation of paired pectoral fins locomotion of labriform fish applied to a fish robot. *Journal of Bionic Engineering*, 2009, **6**, 37–45.

[19] Liu B, Xu M, Wang L, Yang J, Zhang S. Fluid-structure interaction study on a flexible robotic pectoral fin. *IEEE International Conference on Mechatronics and Automation*, Chengdu, China, 2012, 220–225.

[20] Hu T, Shen L, Lin L, Xu H. Biological inspirations, kine-matics modeling, mechanism design and experiments on an undulating robotic fin inspired by *Gymnarchus niloticus. Mechanism and Machine Theory*, 2009, **44**, 633–645.

[21] Zhang Y, He J, Low K H. Parametric study of an underwater finned propulsor inspired by bluespotted ray. *Journal of Bionic Engineering*, 2012, **9**, 166–176.

[22] Tangorra J L, Phelan C, Esposito C, Lauder G V. Use of biorobotic models of highly deformable fins for studying the mechanics and control of fin forces in fishes. *Integrative and Comparative Biology*, 2011, **51**, 176–189.

[23] Yan Q, Zhang S, Yang J. Initial implementation of basic actuated unit of a flexible pectoral fin driven by SMA. *IEEE International Conference on Mechatronics and Automation*, Xi'an, China, 2010, 899–904.

[24] Yan Q, Han Z, Zhang S, Yang J. Parametric research of experiments on a carangiform robotic fish. *Journal of Bionic Engineering*, 2008, **5**, 95–101.

[25] Lin L, Xie H, Zhang D, Shen L. Supervised neural Q_learning based motion control for bionic underwater robots. *Journal of Bionic Engineering*, 2010, **7**, 177–184.

[26] Oyekan J, Lu B, Hu H, Gu D. Using CFD in robotic simulators for pollution monitoring. *3rd Computer Science and Electronic Engineering Conference*, Colchester, UK, 2011, 92–97.

[27] Liu J, Hu H. Biological inspiration: from carangiform fish to multi-joint robotic fish. *Journal of Bionic Engineering*, 2010, **7**, 35–48.

[28] Liang Y, Lee H, Lim S, Lin W, Lee K, Wu C. Proper orthogonal decomposition and its applications. Part 1. Theory. *Journal of Sound and Vibration*, 2002, **252**, 527–544.

[29] Oppenheim A V, Willsky A S, Nawab S H. *Signals and Systems*, 2nd ed, Prentice Hall, Upper Saddle River, NJ, USA, 1997.

[30] Lauder G V, Madden G A, Tangorra J L, Anderson E, Baker T V. Bioinspiration from fish for smart material design and function. *Smart Materials and Structures*, 2011, **20**, 094014.

[31] Gonzalez R C, Woods R E. *Digital Image Processing*, 2nd ed, Prentice Hall, Upper Saddle River, NJ, USA, 2002.

[32] Wang L, Liu B, Xu M, Yang J, Zhang S. Kinematics study on pectoral fins of Koi Carp by digital image processing. *IEEE International Conference on Robotics and Biomimetics*, Guangzhou, China, 2012, 526–531.

[33] Urtasun R, Fua P, Glardon P, Thalmann D. *Mahalanobis Motion Generation*, Report, No: IC/2004/13, 2004.